RSC Advances

PAPER

View Article Online
View Journal | View Issue

Cite this: *RSC Adv.*, 2020, **10**, 16776

Controllable growth of three-dimensional CdS nanoparticles on TiO_2 nanotubes to enhance photocatalytic activity†

Guo-Min Liu,[a] Wen-Yuan Jia,[a] Qiu-Shi Jiang[b] and Zhi-Qiang Cheng *[b]

Exploiting photocatalysts with characteristics of low cost, high reactivity and good recyclability is a great significance for environmental remediation and energy conversion. Herein, hollow TiO_2 nanotubes were fabricated by a novel and efficient method *via* electrospinning and an impregnation calcination method. With the hydrothermal method, the CdS nanoparticles were modified on the surface and in walls of the TiO_2 nanotubes. By changing the reaction conditions, the morphology of CdS nanoparticles presents a controllable three-dimensional (3D) structure. The morphology of the samples was characterized by scanning electron microscopy (SEM) and transmission electron microscopy (TEM). The structure and components of samples were characterized by X-ray diffraction (XRD), energy dispersive X-ray analysis (EDX) and X-ray photoelectron spectroscopy (XPS). The light absorption efficiency was detected using UV-vis diffuse reflectance spectroscopy (DRS) and photoluminescence (PL). The photocatalytic properties were evaluated by degradation of methyl orange (MO) and photocatalytic hydrogen evolution under visible light irradiation. From the results, the TiO_2/CdS nanotubes exhibit better photocatalytic activity than the pure TiO_2. The synthetic mechanism of TiO_2/CdS heterostructures and a possible photocatalytic mechanism based on the experimental results were proposed.

Received 16th January 2020
Accepted 6th April 2020

DOI: 10.1039/c9ra10895e

rsc.li/rsc-advances

1 Introduction

With progress in the field of nanotechnology, it has become possible to prepare semiconducting materials of nanocrystal structures with special shapes and dimensions, such as nanofibers, nanorods, nanoflowers, nanospheres and nanotubes,[1–5] which have garnered extensive attention on account of their unique electronic, optical, and photoactive properties.[6–9] Meanwhile, they are widely utilized in the fields of gas sensors, optical devices, visible light detectors, and field emission emitters, especially for photocatalysis.[10–15] Among copious inorganic semiconductor nanostructures, titanium oxide (TiO_2) has been extensively studied to date, with extensive research on its high surface-to-volume ratio, low cost, environmental friendliness and unique physical and chemical properties.[16–19] Recently, the application of TiO_2 as photocatalysts for degradation of toxic organic pollutants have attracted wide public attention, because the TiO_2 nanostructure and its composites can significantly improve the photocatalytic performance.[20–22] The properties of nanomaterials mainly rely on their nanoscale and morphology, for nanoscale semiconductor to perform well as catalysts, they at least satisfy three characteristics: (1) high specific surface area, (2) have good stability and (3) the size and distribution should be uniform.[23–25] Therefore, TiO_2 nanotubes shows intrinsic advantages compared to traditional TiO_2 in terms of size and specific surface area,[26] design and fabricate TiO_2 based nanotubes for heterogeneous photocatalysis have become a hot research topic. Thus far, many synthesis methods such as electrodeposition method, sol–gel method, template-assisted and hydrothermal treatment, have been developed for fabricating TiO_2 nanotube.[18,19,27,28] However, these traditional method often accompanied problems such as cumbersome operation, template hard removal, high production cost and poor structural stability, *etc.*[29]

Meanwhile, the high recombination rate of photogenerated (PG) electron/hole pairs is another limits factor of photocatalysis.[30,31] Although reduce the size of nanoscale TiO_2 open a convenient way for improving photocatalytic efficiency, but it cannot tackle the fundamental limits issue.[32,33] By contrast, making TiO_2 doped with other elements, modified with noble metal and combined with other semiconductors to form heterostructures, which provide a effective means to inhibit the recombination of PG electron/hole pairs.[34–38] It is necessary to design new-type composite photocatalysts not only improve the separation of PG electron/hole pairs, but also extend the optical absorption of TiO_2, thus to obtain a more efficient utilization of solar energy.[39,40] Cadmium sulfide (CdS) is an excellent n-type

[a]*Department of Orthopedics, The Second Hospital of Jilin University, Changchun 130000, China*

[b]*College of Resources and Environment, Jilin Agriculture University, Changchun 130118, China. E-mail: czq5974@163.com*

† Electronic supplementary information (ESI) available. See DOI: 10.1039/c9ra10895e

semiconductor with an ideal band-gap energy of 2.4 eV, which could absorb the visible light radiation up to 520 nm,[41,42] has been widely used as a visible light response sensitizer.[34,43] By comparing the energy levels of TiO_2 with CdS, which could find their analogical band structures are quite suitable to construct heterostructures and bring an effective separation of PG electron/hole pairs.[44,45] Therefore, that is expected to combination the TiO_2 with CdS form a heterostructure structure for overcoming the demerits that exist in TiO_2 and CdS simultaneously.[46]

Herein, we described the fabrication of CdS decorated TiO_2 nanotubes *via* electrospinning combined with controlled calcination and hydrothermal process. By changing the synthesis condition, the density and size of CdS on the surface (inner wall) of the TiO_2 nanotubes can be controlled. The morphology and dimension of the CdS/TiO_2 nanotubes were observed by the SEM and TEM. The crystal phases, optical absorption properties, elemental and chemical state were explored by XRD, DRS and XPS. Due to the formation of CdS/TiO_2 heterojunction structure, the hybrid nanoparticles could reduce the recombination of PG electron–hole pairs, and the hollow nanotubes structure provides a larger specific surface area and more active sites, that the as-prepared CdS/TiO_2 nanotubes significantly improved photocatalytic activity. Moreover, that may provide a new method for preparation of semiconductor heterostructure nanotubes.

2 Experimental

2.1 Materials

Polystyrene (PS, $M_w \approx 350\,000$ g mol^{-1}), tetrabutyltitanate (TBOT, 97%), cadmium nitrate [$Cd(NO_3)_2 \cdot 4H_2O$, 99%], thiourea (CH_4N_2S, 99%), absolute ethanol (C_2H_6O, 99%), *N*,*N*-dimethylformamide (DMF, 99%), and methyl orange (MO, 96%) were purchased from Aladdin; all of chemicals used in the experiments were analytical grade and used without further purification.

2.2 Methods

The precursor solution was prepared by adding 1.4 g PS to 5.0 mL DMF with magnetic stirring at 50 °C. After PS dissolution in the DMF completely, the prepared solution was loaded into a syringe, which was connected to a 15 kV high voltage. The flow rate of the solution was controlled at 0.5 mL h^{-1}, and the distance from needle to the rotate acceptor was 20 cm. The whole process was kept with humidity below 20%. Then, the PS membrane were soaked in the BOT/ethanol (volume ratio 1 : 10) precursor solution for 5 min. Then, the composite TBOT/PS precursor fibers were natural air dried. Finally, the precursor fibers were calcined to 550 °C with a rate of 2 °C min^{-1} and keep 550 °C for 2 hours, to burn the PS templates completely. After annealing, the hollow TiO_2 nanotubes were obtained.

Hydrothermal method was used for CdS nanoparticles modified. The as prepared TiO_2 nanotubes were transferred into a Teflon-lined autoclave, which containing 30 mL solution of $Cd(NO_3)_2$ and thiourea, the concentration are equal and both volumes are 15 mL. Then, the Teflon-lined autoclave was heated to 200 °C and keep 8 hours. Finally, the CdS/TiO_2 nanotubes were collected and washed in DI water. For compare the effect of reactant concentration on morphology, change the concentration of $Cd(NO_3)_2$ solution to 5, 10, 20, 30 mmol L^{-1} and the corresponding CdS/TiO_2 nanotubes was named as TC1, TC2, TC3 and TC4, respectively (Fig. 1).

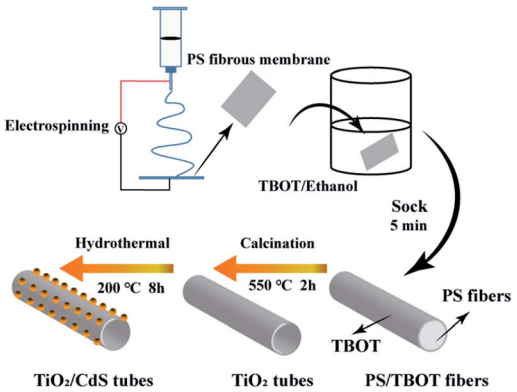

Fig. 1 An illustration of the formation mechanism of the TiO_2/CdS nanotubes.

2.3 Measurement of photocatalytic activity

Methyl orange (MO) was used as the target substrates for evaluating the photocatalytic activity. The photocatalytic reaction was carried out in a reactor with a circulating water system to maintain a constant temperature. The xenon lamp (Philips, 100 W) equipped with a 420 nm cut-off filter instead and the irradiation time were ranged from 5 to 200 min. Under the same conditions, all samples were placed in the quartz tube, which away from the irradiation source 5 cm. The degradation ratio was 40 mL MO solution (10 mg L^{-1}) with 40 mg photocatalyst. Then, the suspension was stirred in the dark for 1 hour to establish adsorption and desorption equilibrium. During the photoreaction process, approximately 3 mL of the mixture was sampled in a constant time, and use centrifugation to separate the nanoparticles. The, using the spectrophotometer to determination the solution concentration. H_2 evolution reactions were proceed in a closed gas-circulation system. 50 mg samples were dispersed in 200 mL aqueous solution of Na_2S (1.0 M) and Na_2SO_3 (1.0 M). After removing the air of reaction system, the solution were irradiated by a 100 W xenon lamp equipped with a 420 nm cut-off filter, and the amount of H_2 were measured by gas chromatography (GC-9700, N_2 carrier).

3 Results and discussion

3.1 XRD patterns

Fig. 2 present the XRD pattern of the as-prepared photocatalysts. The sharp and strong diffraction peaks showed the nanotubes were well crystallized. The main diffraction peaks of TiO_2 were located at 25.45°, 37.95°, 48.20°, 55.16° and 62.81° can be indexed to the (101), (004), (200), (211) and (204) directions, respectively, which indicates that the prepared titanium oxide belongs to the

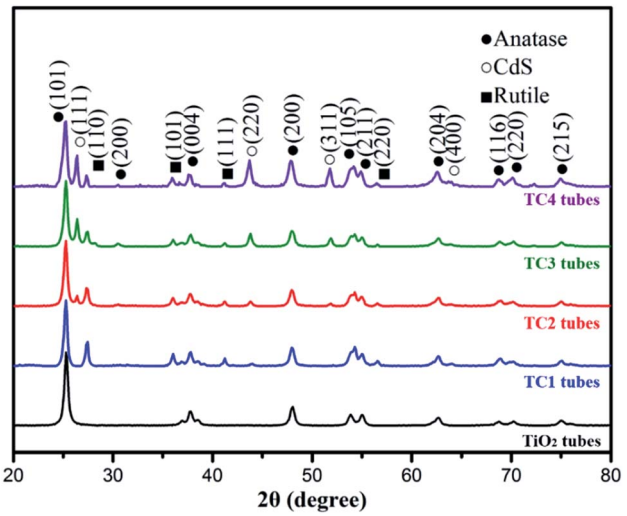

Fig. 2 The XRD patterns of the as-prepared photocatalysts.

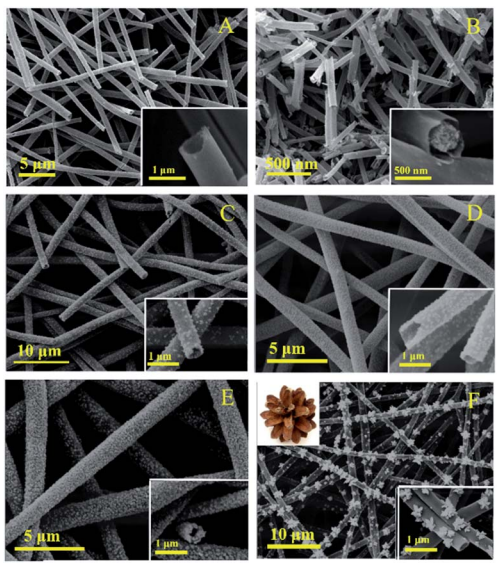

Fig. 3 The SEM images of the samples: (A) TiO_2 nanotubes, (B) core–shell structure TiO_2 nanotubes, (C) TC1 nanotubes, (D) TC2 nanotubes, (E) TC3 nanotubes and (F) TC4 nanotubes.

anatase structure (JCPDS 21-1272), and with a high purity. Compared with pure TiO_2, the CdS/TiO_2 nanotubes can observe the peak at 26.52°, 43.72° confirms the formation of CdS peaks (JCPDS 65-2280), and the peaks were enhanced with increased Cd^{2+} concentration. Meanwhile, there is also a certain amount of rutile phase at 27.2° in the all CdS/TiO_2 nanotubes. Compared the main diffraction pattern of three CdS/TiO_2 nanotubes, the peaks of rutile show an decreased trend due to the addition of Cd^{2+}, which mean the rutile may be an intermediate form of CdS/TiO_2 heterogeneous structure.

3.2 Morphology of electrospun nanotubes TiO_2/CdS

The morphology of the nanotubes were characterized by SEM. Fig. 3A show the SEM image of TiO_2, which are composed by regular and uniform nanotubes with diameter of approximately 700 nm and the uniformity was above 80%, demonstrating the TBOT/ethanol solution permeate into the surface of the PS template fibers successful. From the illustration of Fig. 3A, we can observe the high magnification SEM of a TiO_2 nanotube that present the wall thickness of the nanotube about 100 nm and the inwall of the nanotubes are rough. Fig. 3B clearly present the SEM image of core–shell structure TiO_2 nanotubes, which was obtained by replacing PS/DMF solution with PAN/DMF solution (PAN: 13 wt%) and other operations were the same. The core might be carbon fibers which produced by the PAN incomplete calcination. The SEM of four kinds of CdS/TiO_2 hybrid showed in the Fig. 3C–F with low and high magnifications. Compared to the pure TiO_2 nanotubes, the CdS/TiO_2 nanotubes could observed amount of nanoparticles deposited on the surface and inwall, and the density of nanoparticles increase with the concentration of Cd^{2+} ions. These results show that the morphology of CdS modified on the nanotubes was related to the solution concentration. Notably, further increase of Cd^{2+}, the CdS nanoparticles grown together to form a pine-cone shaped 3D structure as shown in Fig. 3F. The morphology and microstructure of as-prepared photocatalysts also investigated by TEM. The low magnification TEM image (Fig. 4B) further verifies that CdS nanoparticles were well covered the surface and inwall of TiO_2 nanotubes, compared to the TEM of TiO_2 nanotubes (Fig. 4A). These nanoparticles with sizes of 5–50 nm are distributed randomly on the TiO_2. The high resolution TEM image (Fig. 4D) clearly reveals an intimate interface between the TiO_2 and CdS in the composite to form heterojunctions, which is favorable for the electron transfer in photocatalytic activity. Also demonstrates the CdS/TiO_2 photocatalyst obtained by hydrothermal method form a heterostructure rather than a mixture of TiO_2 and CdS. Meanwhile, the

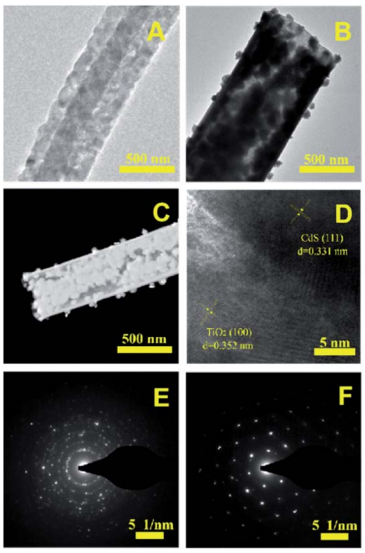

Fig. 4 The TEM image of TiO_2 nanotubes (A) and TC3 nanotubes (B), the STEM image of TC3 nanotubes (C) and the HRTEM of TC3 nanotubes (D), the SAED pattern of the TC3 (E) and the CdS Nps of the surface of TC3 (F).

high resolution TEM are carried out to survey the lattice fringes of CdS/TiO_2 nanotubes, the lattice spacing are 0.35 nm and 0.33 nm, which are coincident with the (101) spacing of anatase TiO_2 and (111) of CdS phase. The legible fringe also suggests the high degree of crystallinity corresponds with the result of XRD results. The Fig. 4E illustrates the selected area electron diffraction (SAED) pattern of TiO_2/CdS, which presentation a bright diffraction rings assigned to high crystallization and polycrystalline structure. The Fig. 4F was SAED pattern of pure CdS nanoparticles on the surface of TC3 means the obtained CdS particles were pure single crystals.

3.3 XPS analysis

XPS analyze could reveal the information about the surface composition and chemical state. As shown in Fig. 5A, CdS/TiO_2 hybrid (TC2) is mainly composed of five elements, which is Ti, O, Cd, S and C, The peak of C 1s can be ascribed to the hydrocarbon from the instrument itself. The high resolution spectra of Ti 2p were exhibited in the Fig. 5B. The Ti 2p spectra shows the peaks at 458.3 eV and 464.1 eV for Ti $2p_{3/2}$ and Ti $2p_{1/2}$ of TiO_2, respectively. The distance between the two peaks is 5.8 eV, which is identical to that of the neat TiO_2 indicating that Ti ion is in the form of Ti^{4+}, high resolution spectrum of Cd 3d (Fig. 4C) displayed characteristic peaks of 404.5 eV and 411.4 eV, which are corresponding to the Cd $3d_{5/2}$ and Cd $3d_{3/2}$ states of Cd^{2+} in CdS, respectively. Consequently, XPS analysis further determines the formation of TiO_2 and CdS in the sample, which is agreement with XRD and TEM result.

3.4 UV-vis diffuse reflection spectra and PL spectra

UV-vis DRS are tested to determine the optical properties of the photocatalysts. From the results of DRS (Fig. 6A) the reflection spectra of TiO_2 and CdS/TiO_2 heterostructure in the region

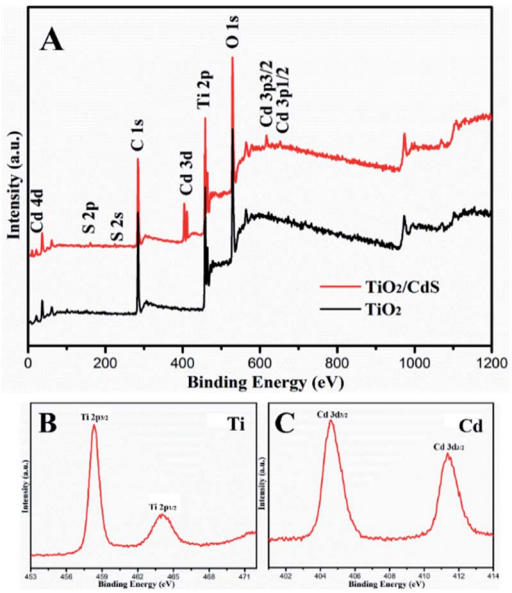

Fig. 5 The XPS spectra of the TiO_2 and TC3 nanotubes: full spectrum of the sample (A), the Ti 2p spectrum (B) and Cd 3d spectrum (C).

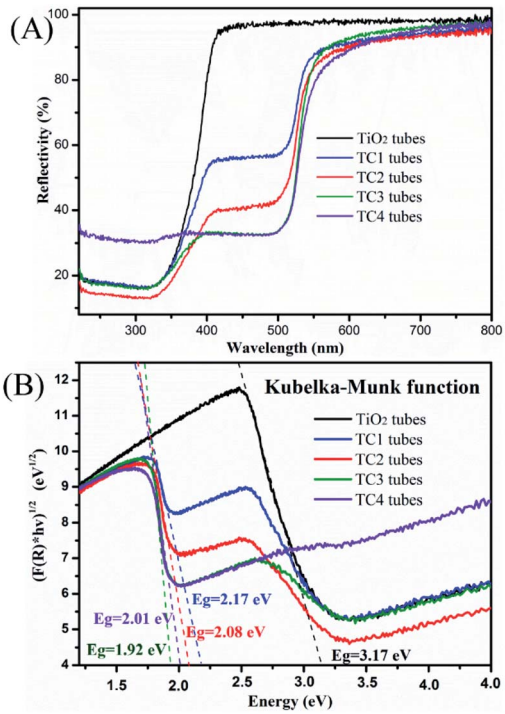

Fig. 6 (A) The UV-vis diffuse reflection spectra (DRS) of the as-prepared photocatalysts and (B) Kubelka–Munk transformed reflectance spectra.

spanning from 230 to 800 nm were showed. Compared to the TiO_2 nanotubes, the TC2 had a lower reflectivity in the range of 240–380 nm, especially in the ultraviolet light range. After the modified of CdS, all CdS/TiO_2 nanotubes present a remarkable light adsorption into the visible light region, which may due to the excellent visible-light photoresponse of CdS nanoparticles. Notably, the adsorption edges of CdS/TiO_2 nanotubes gradually broaden with the mount of modified CdS nanoparticles increasing, indicated the high responsiveness of the photocatalyst to visible light.

Fig. 6B is the forbidden bandwidth obtained by the catalyst according to the Kubelka–Munk formula. Among them, the forbidden band widths of TiO_2 and four CdS/TiO_2 heterostructures (TC1, TC2, TC3 and TC4) are 3.17 eV, 2.17 eV, 2.08 eV, 1.92 eV and 2.01 eV. It can be seen from the comparison with the TiO_2 tubes that the forbidden bandwidth of the CdS/TiO_2 heterostructure is significantly reduced. Among them, TC3 has the lowest forbidden bandwidth. We can speculate that this sample has the best catalytic performance, and the catalytic experiments proved that the prediction was correct. (The detailed content of the edge position is Fig. S1.†)

3.5 Photoluminescence analysis

PL spectroscopy is correlation with the separation and recombination of PG electrons/holes. As shown in Fig. 7, the PL spectra of the TiO_2 nanotubes showed a strong emission peak at 390 nm (excitation wavelength: 370 nm). However, the PL peak intensity of CdS/TiO_2 nanotubes was significantly decreased

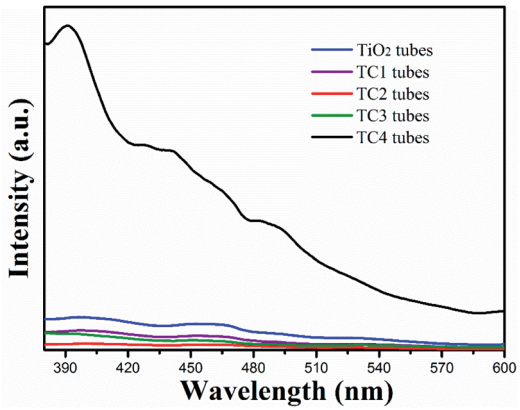

Fig. 7 The photoluminescence spectra of the as-prepared photocatalysts.

with modification amount of CdS nanoparticles increased. The key factor in the formation of this phenomenon is the defects in the crystal structure of TiO_2, which act as traps for capturing the photo-excited electrons and thus, inhibit the recombination of the electrons and holes pairs.

3.6 Photocatalytic activity and recycled photocatalytic degradation performance

To identify the photocatalytic of the as-prepared samples, MO solution degradation were tested under UV and visible irradiation. The photocatalytic effect was evaluated by C_0/C_t (C_0 nd C_t were the initial concentration and the concentration of MO at time t, respectively). From the Fig. 8A, shows the concentration change of MO in the process of photodegradation, after irradiated by UV light for 30 min, the photocatalytic degradation efficiencies of the TC2 nanotubes are 95.3% slightly better than the TC3 (83.2%), which is much higher than the TC4 (72.5%) and pure TiO_2 nanotubes (37.8%). The photodegradation of MO without catalysis almost negligible. However, as shown in Fig. 8B, under visible light irradiation (λ > 420 nm) for 200 minutes the TC3 shows the excellent visible light catalysis (95.2%) similar to the TC4 (94.7%), which CdS load looks like pine-cone shaped and much higher than TC2 (82.6%), TC1 (61.2%), and pure TiO_2 nanotubes (0.09%), which was consistent with the results of UV-vis DRS. In addition, we also investigated the photocatalytic stability of TiO_2/CdS heterostructure (TC3) under visible light irradiation. The results indicated that the hybrids exhibited good stability after being reused for five times (Fig. 8D).

Meanwhile, the photocatalytic activities of the nanotubes were evaluated by H_2 production experiment under the visible light irradiation in aqueous solution (containing 1.0 M Na_2SO_3 and 1.0 M Na_2S as sacrificial reagents). Fig. 8C shows the H_2 evolution rate by the TiO_2 and TiO_2/CdS nanotubes, and there is no appreciable H_2 was observed when TiO_2 nanotubes was tested. In contrast, the TC1 exhibited a slightly enhanced H_2 evolution rate of 22.35 μmol g^{-1} h^{-1}. With the increase of CdS, the H_2 evolution rate are increased. The H_2 evolution rate of TC2 photocatalyst is 64.26 μmol g^{-1} h^{-1} and TC3 (118.73 μmol g^{-1} h^{-1}) reaches a maximum H_2 evolution rate, demonstrates that is effective to employ CdS as cocatalyst for improving efficiency of TiO_2 photocatalytic activity. Further increases the amount of modification of CdS, the H_2 generation rate (TC4 112.86 mol g^{-1} h^{-1}) showed a slight decrease. This might be due to the less exposed active sites of TiO_2/CdS resulting from the excess CdS shielding.

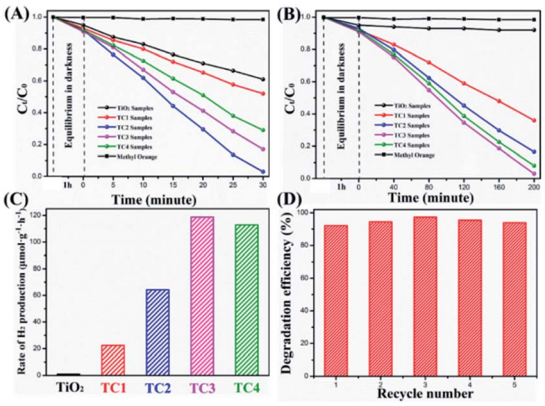

Fig. 8 Degradation rates of as-prepared photocatalysts under the UV-light (A); degradation rates of as-prepared photocatalysts under the visible light (B); the rate of H_2 evolution on TiO_2/CdS nanotubes under visible light (C); the repeatability tests studied on the TC3 nanotubes for five recycles (D).

3.7 Mechanism for the enhancement of photocatalytic activity

The principle of photocatalytic decomposition over CdS/TiO_2 heterostructure is delineated in Fig. 9. Under the visible-light irradiation, the charge carriers were firstly generated from CdS owing to its narrow energy band gap. The photoexcited electrons on the valence band (VB) of CdS can move to their own conduction band (CB). However, the high recombination of electrons (e^-) and holes (h^+) of CdS limits its photocatalytic activity. When the TiO_2 and CdS form a heterostructure, the PG e^- on CdS nanoparticles can easily transfer to the CB of TiO_2 through the interface as a result of the lower conduction edge

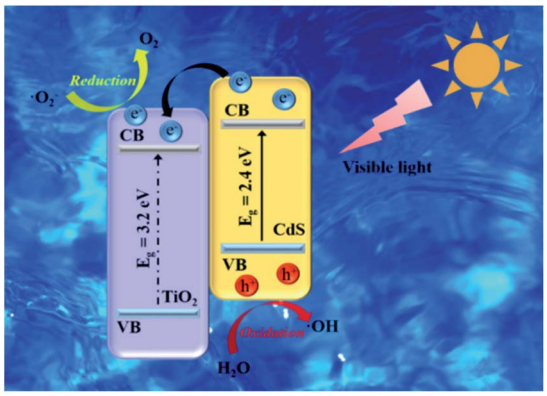

Fig. 9 Schematic diagram for the photocatalytic mechanism of the TiO_2/CdS catalysts under visible-light irradiation.

potential of TiO_2 than that of CdS. Meanwhile, the h^+ remain on the VB of CdS. Therefore, the TiO_2 acts as a temporary e^- trap to decrease the recombination of PG e^-/h^+. Consequently, the PG h^+ on the VB of CdS can react with the surface adsorbed H_2O to generate $\cdot OH$. The e^- on the CB of TiO_2 could reduce the adsorbed O_2 to form $\cdot O_2^-$. Organic dye (MO) are eventually oxidized by these highly active species to CO_2 and H_2O products. The major reaction steps are revealed as follows:

$$TiO_2/CdS + hv \rightarrow TiO_2/CdS\ (e^- + h^+) \quad (1)$$

$$TiO_2/CdS\ (e^- + h^+) \rightarrow TiO_2\ (e^-) + CdS\ (h^+) \quad (2)$$

$$e^- + O_2 + \rightarrow \cdot O_2^- \quad (3)$$

$$e^- + \cdot O_2^- + H^+ \rightarrow \cdot OH + OH^- \quad (4)$$

$$h^+ + H_2O \rightarrow \cdot OH \quad (5)$$

$$\cdot OH + \text{organic} \rightarrow \text{other products} \rightarrow CO_2 + H_2O \quad (6)$$

4 Conclusions

In summary, hollow TiO_2 nanotubes were obtained using electrospinning combined with an impregnation calcination method. CdS nanoparticles were modified on the surface and inner wall of TiO_2 nanotubes *via* hydrothermal process. By changing the reaction conditions, the size and density of CdS on the surface and inner wall of the TiO_2 nanotubes can be controlled. Owing to the formation of heterojunction structure, the hybrid nanoparticles could enhanced separation of e^-/h^+ pairs and reduce the recombination of charge carriers, and the hollow nanotubes structure provides a larger specific surface area and more active sites, that the CdS/TiO_2 nanotubes showed remarkably photocatalytic activity than pure TiO_2. Moreover, that may provide a new method for preparation of heterostructure nanotubes.

Conflicts of interest

No conflicts of interest in this article.

Acknowledgements

This study was supported by the Special Health Project of Jilin Province, China (No. 3D516D703429) and the Special Health Project of Department of Finance of Jilin Province, China (No. 3D5177703429).

References

1 L. Zhang, Z. Q. Cheng, D. F. Wang and J. F. Li, *Mater. Lett.*, 2015, **158**, 439–441.
2 G. Jiang, R. Wang, X. Wang, X. Xi, R. Hu, Y. Zhou, S. Wang, T. Wang and W. Chen, *ACS Appl. Mater. Interfaces*, 2012, **4**, 4440–4444.
3 J. N. Li, Z. Q. Cheng, M. Z. Liu, M. Y. Zhang, M. J. Hu, L. Zhang, H. F. Jiang and J. F. Li, *J. Appl. Polym. Sci.*, 2015, **132**, 41627–41635.
4 J. Di, J. X. Xia, M. X. Ji, B. Wang, X. W. Li, Q. Zhang, Z. G. Chen and H. M. Li, *ACS Sustainable Chem. Eng.*, 2016, **4**, 136–146.
5 R. Zamiri, B. Singh, M. S. Belsley and J. M. F. Ferreira, *Ceram. Int.*, 2014, **40**, 6031–6036.
6 W. Tian, T. Y. Zhai, C. Zhang, S. L. Li, X. Wang, F. Liu, D. Q. Liu, X. K. Cai, K. Tsukagoshi, D. Golberg and Y. Bando, *Adv. Mater.*, 2013, **25**, 4625–4630.
7 Z. Q. Cheng, S. Z. Zhao, L. J. Kang, M. T. Li and Z. L. Gao, *Mater. Lett.*, 2018, **214**, 80–83.
8 Y. A. Zhang, C. X. Wang, Z. M. Yuan, L. Y. Zhang and L. W. Yin, *Eur. J. Inorg. Chem.*, 2017, 2281–2288, DOI: DOI: 10.1002/ejic.201601535.
9 Q. Tang, X. F. Meng, Z. Y. Wang, J. W. Zhou and H. Tang, *Appl. Surf. Sci.*, 2018, **430**, 253–262.
10 H. Chen, X. X. Wang, J. X. Li and X. K. Wang, *J. Mater. Chem. A*, 2015, **3**, 6073–6081.
11 J. M. Du, H. M. Wang, M. K. Yang, K. D. Li, L. X. Zhao, G. Y. Zhao, S. J. Li, X. L. Gu, Y. L. Zhou, L. Wang, Y. T. Gao, W. M. Wang and D. J. Kang, *Electrochim. Acta*, 2017, **250**, 99–107.
12 S. H. Hwang, J. Song, Y. Jung, O. Y. Kweon, H. Song and J. Jang, *Chem. Commun.*, 2011, **47**, 9164–9166.
13 B. X. Li, B. S. Zhang, S. B. Nie, L. Z. Shao and L. Y. Hu, *J. Catal.*, 2017, **348**, 256–264.
14 D. Lin, H. Wu and W. Pan, *Adv. Mater.*, 2007, **19**, 3968–3972.
15 J. A. Park, J. Moon, S. J. Lee, S. H. Kim, H. Y. Chu and T. Zyung, *Sens. Actuators, B*, 2010, **145**, 592–595.
16 F. L. Zhang, Z. Q. Cheng, L. J. Kang, L. Y. Cui, W. Liu, X. J. Xu, G. H. Hou and H. J. Yang, *RSC Adv.*, 2015, **5**, 32088–32091.
17 X. F. Wang, O. Kitao, E. Hosono, H. S. Zhou, S. Sasaki and H. Tamiaki, *J. Photochem. Photobiol., A*, 2010, **210**, 145–152.
18 J. T. Yan, S. Y. Gao, C. L. Wang, B. Chai, J. F. Li, G. S. Song and S. Z. Chen, *Mater. Lett.*, 2016, **184**, 43–46.
19 C. S. Niu, J. S. Meng, X. P. Wang, C. H. Han, M. Y. Yan, K. N. Zhao, X. M. Xu, W. H. Ren, Y. L. Zhao, L. Xu, Q. J. Zhang, D. Y. Zhao and L. Q. Mai, *Nat. Commun.*, 2015, **6**, 7402–7410.
20 F. X. Xiao, *ACS Appl. Mater. Interfaces*, 2012, **4**, 7054–7062.
21 F. L. Zhang, Z. Q. Cheng, L. Y. Cui, T. T. Duan, A. Anan, C. F. Zhang and L. J. Kang, *RSC Adv.*, 2016, **6**, 1844–1850.
22 F. L. Zhang, Z. Q. Cheng, L. J. Kang, L. Y. Cui, W. Liu, G. H. Hou, H. J. Yang and X. J. Xu, *RSC Adv.*, 2014, **4**, 63520–63525.
23 D. D. Lin, H. Wu, R. Zhang and W. Pan, *Chem. Mater.*, 2009, **21**, 3479–3484.
24 G. H. Hou, Z. Q. Cheng, L. J. Kang, X. J. Xu, F. L. Zhang and H. J. Yang, *Crystengcomm*, 2015, **17**, 5496–5501.
25 S. Z. Zhao, Z. G. Cheng, L. J. Kang, Y. Y. Zhang and X. D. Zhao, *Mater. Lett.*, 2016, **182**, 305–308.
26 J. J. Liu and B. Cheng, *Appl. Surf. Sci.*, 2018, **430**, 348–354.
27 D. Yang, H. J. Zou, Y. Z. Wu, J. F. Shi, S. H. Zhang, X. D. Wang, P. P. Han, Z. W. Tong and Z. Y. Jiang, *Ind. Eng. Chem. Res.*, 2017, **56**, 6247–6255.

28 C. L. Wang, X. Tan, J. T. Yan, B. Chai, J. F. Li and S. Z. Chen, *Appl. Surf. Sci.*, 2017, **396**, 780–790.
29 Y. P. Huang, Y. E. Miao, L. S. Zhang, W. W. Tjiu, J. S. Pan and T. X. Liu, *Nanoscale*, 2014, **6**, 10673–10679.
30 J. P. Wang, J. K. Cong, H. Xu, J. M. Wang, H. Liu, M. Liang, J. K. Gao, Q. Q. Ni and J. M. Yao, *ACS Sustainable Chem. Eng.*, 2017, **5**, 10633–10639.
31 X. J. Zhou, C. L. Shao, X. H. Li, X. X. Wang, X. H. Guo and Y. C. Liu, *J. Hazard. Mater.*, 2018, **344**, 113–122.
32 S. Z. Zhao, Z. Q. Cheng, L. J. Kang, M. T. Li and Z. L. Gao, *RSC Adv.*, 2017, **7**, 50064–50071.
33 X. J. Zhou, G. Zhang, C. L. Shao, X. H. Li, X. Jiang and Y. C. Liu, *Ceram. Int.*, 2017, **43**, 15699–15707.
34 L. Wu, J. C. Yu and X. Z. Fu, *J. Mol. Catal. A: Chem.*, 2006, **244**, 25–32.
35 N. Irannejad, B. Rezaei, A. A. Ensafi and M. M. Momeni, *Electrochim. Acta*, 2017, **247**, 764–770.
36 B. X. Li, Y. G. Hao, B. S. Zhang, X. K. Shao and L. Y. Hu, *Appl. Catal., A*, 2017, **531**, 1–12.
37 H. Wei, W. A. McMaster, J. Z. Y. Tan, L. Cao, D. H. Chen and R. A. Caruso, *J. Phys. Chem. C*, 2017, **121**, 22114–22122.
38 J. Gao, Y. Zhou, Z. S. Li, S. C. Yan, N. Y. Wang and Z. G. Zou, *Nanoscale*, 2012, **4**, 3687–3692.
39 Z. Q. Cheng, S. Z. Zhao, Z. L. Han, Y. Y. Zhang, X. D. Zhao and L. J. Kang, *Crystengcomm*, 2016, **18**, 8756–8761.
40 H. Wang, Y. H. Liang, L. Liu, J. S. Hu and W. Q. Cui, *J. Hazard. Mater.*, 2018, **344**, 369–380.
41 J. Fu, G. N. Li, F. N. Xi and X. P. Dong, *Chem. Eng. J.*, 2012, **180**, 330–336.
42 J. R. Ran, J. G. Yu and M. Jaroniec, *Green Chem.*, 2011, **13**, 2708–2713.
43 B. Pant, M. Park, H. Y. Kim and S. J. Park, *J. Alloys Compd.*, 2017, **699**, 73–78.
44 F. Y. Tian, D. F. Hou, F. C. Hu, K. Xie, X. Q. Qiao and D. S. Li, *Appl. Surf. Sci.*, 2017, **391**, 295–302.
45 J. Fu, B. B. Chang, Y. L. Tian, F. N. Xi and X. P. Dong, *J. Mater. Chem. A*, 2013, **1**, 3083–3090.
46 Y. L. Tian, J. Fu, B. B. Chang, F. N. Xi and X. P. Dong, *Mater. Lett.*, 2012, **81**, 95–98.